Contribution of moderate climate events to atoll island building (Fakarava Atoll, French Polynesia)

Virginie Duvat, Valentin Pillet, Natacha Volto, Heitea Terorotua, Victoire Laurent

Contribution of moderate climate events to atoll island building (Fakarava, French Polynesia)

1. Introduction

Extreme climate events, including storm-related (i.e. tropical cyclones and distant-source swells) and El Niño- and La Niña-related, are widely acknowledged to play a major role in atoll island change through a complex combination of erosional and accretional processes (Nurse et al., 2014). The effects of tropical cyclones on atoll islands have been extensively investigated since the 1960s, and their contrasting, i.e. both destructive and constructional, impacts highlighted at different spatial-temporal scales (Stoddart, 1969, 1971; Maragos et al., 1973; Baines et al., 1974; Baines and McLean, 1976; Woodroffe, 1983; Scoffin, 1993; Le Cozannet et al., 2013; Ford and Kench, 2014, 2016; Duvat and Pillet, 2017; Duvat et al., 2017a, 2017b). In addition, over the past decade a growing number of studies have reported the impacts of distant-source swells on Pacific and Indian Oceans' atoll islands (Hoeke et al., 2013; Smithers and Hoeke, 2014; Aslam and Kench, 2018; Wadey et al., 2018; Canavesio, 2019). These studies have shown that such events, which had until recently remained poorly understood, also contribute significantly to atoll island change, in particular through overwash-driven processes that cause island erosion and/or building, depending on the context. Together, these studies have underscored that the response of atoll islands to cyclonic and distant-source swells is influenced by human interferences with natural processes, including in particular the removal of the coastal vegetation or the replacement of native species by introduced species (Stoddart, 1963, 1965; Duvat et al., 2017a), the obstruction or reduction in width of inter-islet channels as a result of land reclamation (Canavesio, 2019), and shoreline hardening (Smithers and Hoeke, 2014). Although they have been less investigated, the effects of El Niño and La Niña phases on alongshore sediment transport, and

thereby on shoreline change, have been studied in Kiribati, where Rankey (2011) reported beach migration. Moreover, El Niño events play a major role in the occurrence of tropical cyclones in some ocean regions (e.g. Tuamotu Archipelago, Central Pacific) that are located outside the cyclone belt and are only liable to experience tropical cyclones under El Niño conditions (Larrue and Chirron, 2010). Additionally, some studies have emphasised the major role of tsunami in atoll island building, for example in the Maldives, following the 2004 Sumatra tsunami (Kench et al., 2006). Generally, it can be noted that intense events, either climate- or tectonic-related, have so far been the main focus of atoll geomorphic studies. The influence of moderate climate events, such as tropical lows that do not reach the cyclone stage and low-magnitude distant-source swells, has to date been overlooked. However, because they are much more frequent than extreme climate events, these events can be assumed to contribute significantly to atoll island change, especially in regions where intense climate events are uncommon.

This article addresses this research gap by focusing on a moderate climate event, i.e. tropical low 13F, which affected the northern part of Fakarava Atoll, Tuamotu Archipelago, in February 2017. Based on multi-date image analysis and field observations which were conducted before, immediately after and one year after the event, it demonstrates that moderate climate events significantly contribute to atoll island change. This article especially underscores their constructional effects and the interferences between the physical processes operating during such events and human activities. It then discusses the implications of findings for future research and coastal risk reduction on atoll islands.

2. Context of the study

2.1. Study area

50 The Tuamotu Archipelago is one of the five archipelagos composing French Polynesia (Fig.
51 1) and the largest group of atolls (77) in the world. It is composed of two chains of atolls and
52 stretches >1,500 km from northwest to southeast, extending from 14°21'S to 23°22'S and
53 from 134°28'W to 148°43'W. Fakarava Atoll is located in the northwestern part of the
54 Tuamotu Archipelago at 16°18'S and 145°36'W (Fig. 1), and is the second largest atoll
55 (1.246 km^2) of this archipelago after Rangiroa (1.762 km^2). It exhibits a rectangular shape,
56 measures approximately 54.9 km long from northwest to southeast, and has a maximum width
57 of 24.9 km (Fig. 2a). Fakarava is an open atoll having two passes connecting the open ocean
58 to the lagoon at it northern (Garuae Pass) and southern (Temakohua Pass) extremities. Its
59 lagoon is one of the deepest of the Tuamotu Archipelago, with a maximum depth of
60 approximately 60 m (Rougerie, 1994). The total land area of the islands that have formed on
61 the atoll rim is approximately 27 km^2. The study area is located on the northern part of the
62 atoll rim, and is composed of five islands stretching >14 km between the Garuae Pass, in the
63 central north, and the southern end of the main village, Rotoava, located in the north-eastern
64 angle of the atoll (Fig. 2b). These islands are 180 to 380 m wide and perched on a
65 conglomerate platform which extends by 50 to 100 m seaward from the base of the beach. On
66 their north-facing ocean coast, they exhibit a more or less dense vegetation belt composed of
67 native species (*Pemphis acidula, Suriana maritima, Scaevola taccada, Guettarda speciosa,*
68 *Tournefortia argentea*). The population of Fakarava counted 674 inhabitants in 2017, most of
69 which live in the village (ISPF, 2017).
70 The climate regime of the study area is controlled by the combined influence of the trade
71 winds from the northeast to southeast directions, and of tropical and extra-tropical storms
72 (Andrefouët et al., 2012). In the Austral Summer (November-March), trade winds are weak
73 and generate moderate waves that can be disturbed by storm waves originating either from
74 tropical cyclones (especially during El Niño phases), or from distant storms forming in

northern latitudes. However, like other Tuamotu atolls, Fakarava is rarely affected by tropical cyclones, the return period of which is ~39 years (Larrue and Chiron, 2010). The last tropical cyclone that affected Fakarava was Orama (category 3) in February 1983 (Laurent and Varney, 2014). During the Austral Summer, Fakarava is relatively protected from northern distant-source waves by northern atolls due to the atoll 'shadow effect' (Andrefouët et al., 2012). In the Austral Winter (April-October), the combination of stronger trade winds (northeast-southeast, clockwise) and stronger distant-source southern swells generate more energetic conditions in the western Tuamotu region. During this season, Fakarava is highly exposed to the distant-source swells originating from the south and southwest, as a result of its location at the western border of the Tuamotu Archipelago.

In the western Tuamotu atolls, the mean tidal range is approximately 0.5 m and reaches an average of 0.65 m at spring tide (Pirazzoli and Montaggioni, 1986). Based on the reconstruction of sea levels in the Pacific Island Region over a 60-year time period (1950–2009), Becker et al.

(2012) estimated absolute sea-level rise in the northern Tuamotu region to be 2.5 ± 0.5 mm/y. This rate is higher than the global mean sea-level rise for the twentieth century, which was estimated to be ~1.8 mm/y by Church and White (2011) and 1.2 ± 0.2 mm/y by Hay et al. (2015). This value is comparable to the absolute sea-level rise estimated for the Marshall (1.4±0.6mm/y at Majuro) and Gilbert Islands (2.2±0.6mm/y at Tarawa), but smaller than the maximal rate of 4.7± 0.7 mm/y obtained for Funafuti Atoll in Tuvalu (Becker et al., 2012).

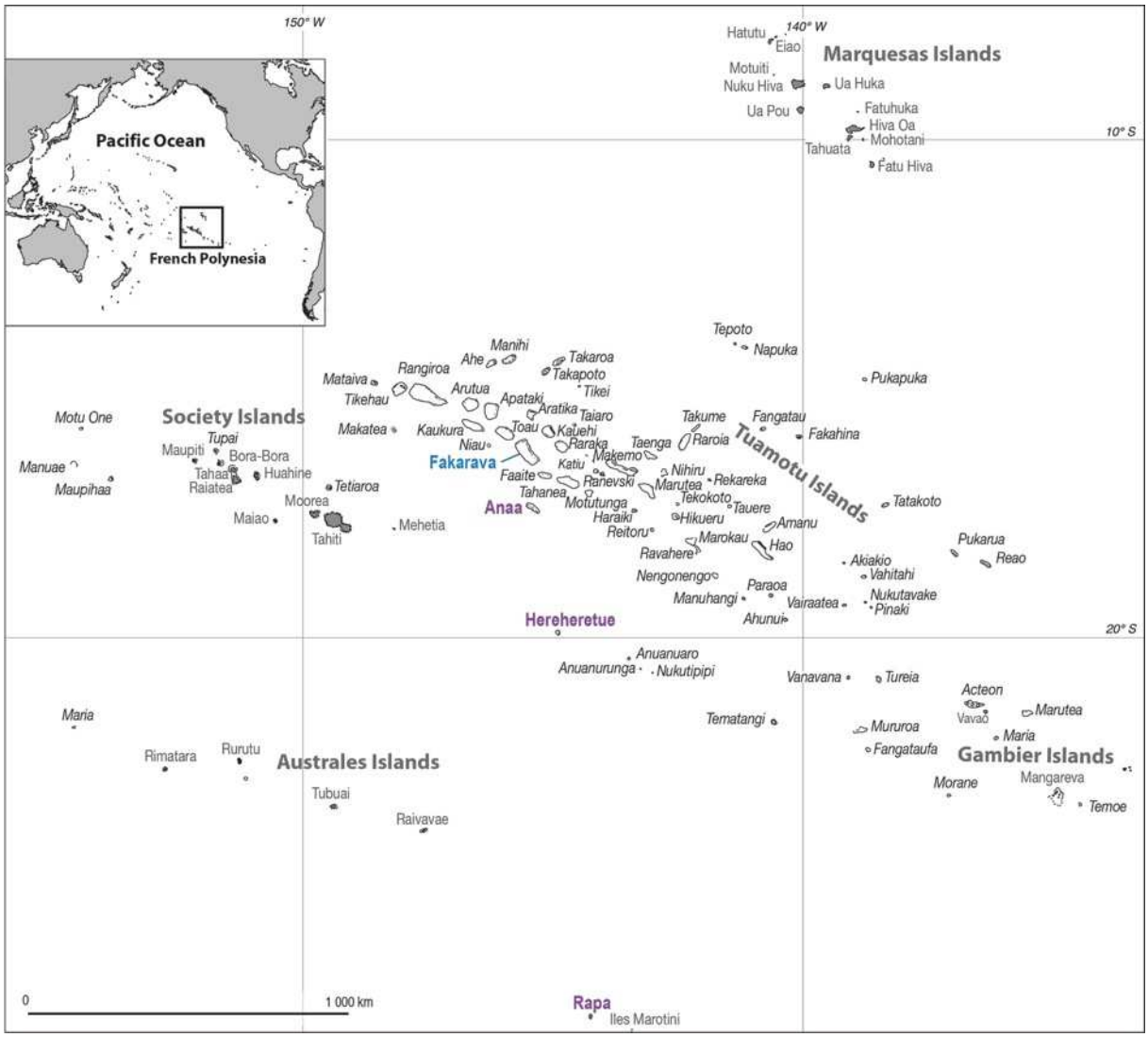

Figure 1. Location map of the study area.

Fakarava Atoll is shown in blue. Other locations mentioned in the text are shown in purple.

2.2. Meteorological event of February 2017

From 13 to 20 February 2017, a tropical low developed within the South Pacific Convergence Zone, which generated strong winds and swells across the northern Tuamotu atolls. Named 13F by the Fiji Meteorological Service on 16 February, it moved on an axis stretching from the Society Islands to the Centre Tuamotu and Australes Islands. On 16 February at 2 pm, French Polynesia time, the tropical low was centred 60 km to the west of Hereheretue, with mean sea level pressure of 999.8 hPa measured on Anaa. It generated northwesterly

maximum sustained 10-mn winds of 74 km/h, with the highest gusts reaching 106 km/h on Hao. These strong winds generated strong swells, with wave height reaching between 4 to 4.9 m at Fakarava and up to 6.1 m between Anaa and Hereheretue. Due to the northwesterly origin of the swells, this event mainly impacted the northwestern and northern sides of the atoll, including the village of Rotoava. The inhabitants of the village estimated that wave height reached up to 4 m on the northeastern ocean coast of the main island (Terorotua, 2017). On Fakarava, the winds and swells caused the cancellation of all flights connecting the atoll to other destinations from 15 February to 19 February. On 17 February, tropical low 13F moved to the south-east of Tahiti, with estimated central pressure of 992 hPa, then to the northeast of Rapa on 18, and eventually left French Polynesia on 19 February. From Gumbel distribution, the return period of such an event is two years from mean sea level pressure (992hPa) and three years from maximum significant wave height (6.1 m).

Compared to the most intense tropical cyclones that have affected the northwestern Tuamotu atolls over the past century – that is, tropical cyclones Orama and Veena, in February and April 1983, respectively – tropical low 13F can be considered a moderate event. For example, tropical cyclone Orama, which severely affected the northwestern atolls of the Tuamotu chain including Fakarava Atoll, exhibited a minimum sea level pressure of 925 hPa, sustained winds of 185 km/h and a maximum wave height of ~9 m on the most exposed (i.e. southern) coast of nearby Rangiroa Atoll (Duvat et al., 2018).

3. Materials and Methods

3.1. Fieldwork

Two field trips allowed to document the morphological impacts of tropical low 13F. The first one took place in February 2017, including immediately before and immediately after the event, as some of the authors were conducting fieldwork on the atoll when the event occurred.

This allowed to make a qualitative assessment of the erosional and accretional geomorphic features generated by this event along 14 km of ocean-facing shoreline between Garuae Pass and the village (see locations on Fig. 2b). This first field trip allowed to directly observe and thus precisely attribute impacts to tropical low 13F, and to comprehend the respective importance of erosional and accretional features in the study area. Additionally, field observations were used to validate the mapping of sediment deposits derived from satellite image analysis (see section 3.2). Observations were made in the intertidal zone, i.e. on the ocean-side reef flat, in hoa (i.e. inter-island channels), in the coastal zone on both ocean and lagoon shores, and in inland areas. This first field trip also allowed to conduct interviews with both local residents living in the impacted area and diving instructors who made direct observations of impacts on the northern outer slopes of the atoll a few days after the event. These interviews allowed to collect information on wave height at the coast, morphological impacts inland (e.g. sediment deposition in properties) and the mechanical destruction of corals on the outer slopes.

The second field trip was conducted from 3 to 10 March 2018, that is, approximately one year after the event, in order to study shoreline readjustment and reef-to-shore sediment transfer resulting from the dismantling of the accretional features that had formed in the intertidal zone during the event. During this field trip, we took Unmanned Aerial Vehicle (UAV) images in areas exhibiting remarkable accretional features, such as storm ramparts (see location in Fig. 2b). This allowed to assess changes in the configuration and position of storm ramparts and sediment transport from the intertidal to the coastal zone between February 2017 and March 2018.

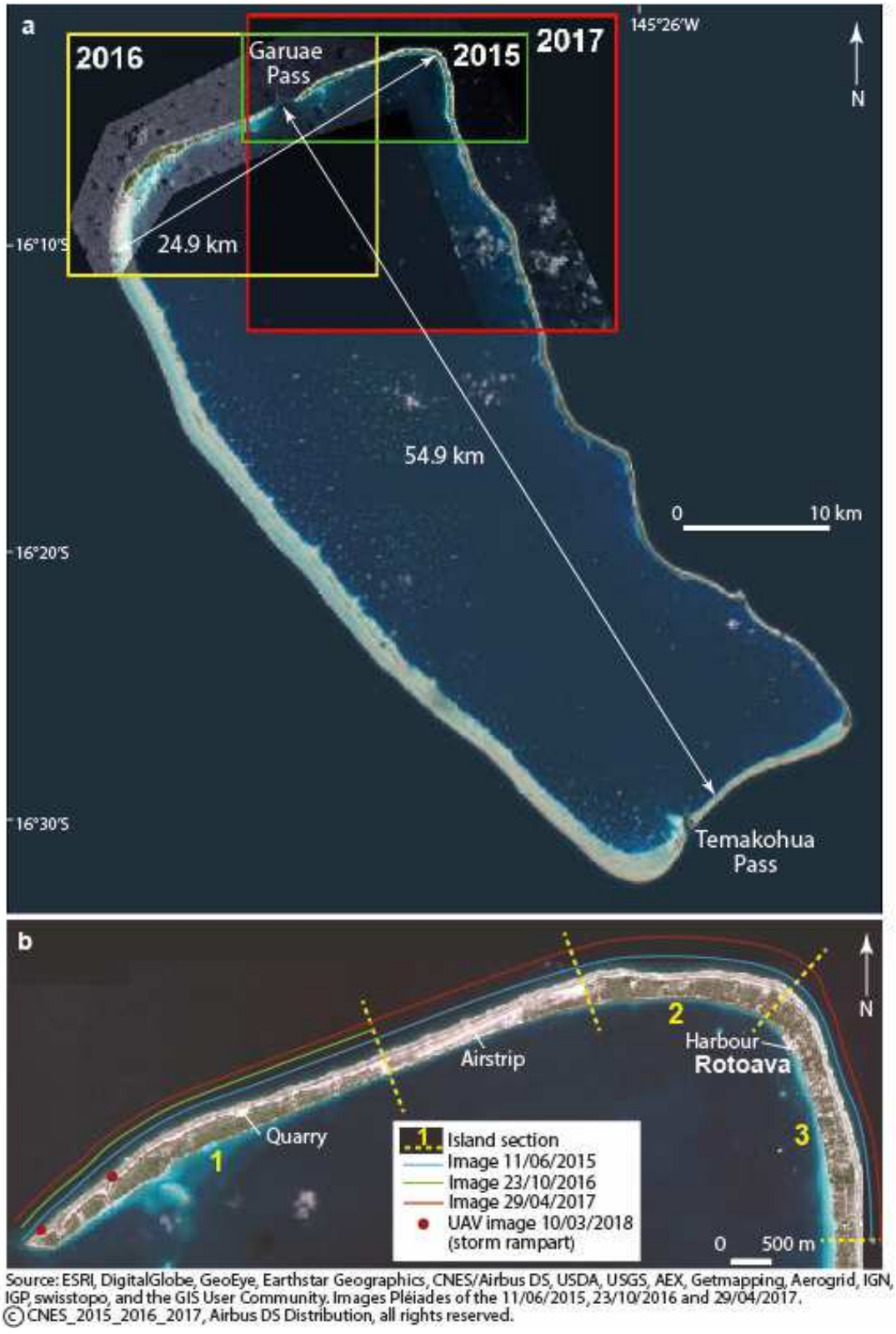

Figure 2. Location of study area and study island sections.

a and b show the coverage of the satellite images used in this study. In a, the green, yellow and red boxes indicate 2015, 2016 and 2017 image coverage, respectively. b shows the subdivision of the study area into three

159 distinct areas (i.e. 1, 2 and 3), and the extent of the no data area (corresponding to the airstrip, excluded from the
160 analysis). It also shows the location of some places of interest cited in the text.
161

162 **3.2. Multi-date satellite image analysis**

163 **3.2.1. Image acquisition and preparation**

164 **Shoreline change analysis**

165 The satellite images used in this study were obtained from Airbus Defence and Space
166 archives. Due to image availability constraints, we had to use two different images to
167 characterise the pre-event situation and to restrict the study area to the northeastern part of the
168 atoll extending from Garuae Pass to the south of the inhabited area (Fig. 2a). The pre-event
169 images were acquired on 11 June 2015 (northeastern part of the atoll, including the inhabited
170 area) and 23 October 2016 (central northern part of the atoll, including Garuae Pass and most
171 of the airstrip), i.e. respectively eight and four months before the event (Table 1). The post-
172 cyclone image was taken on 29 April 2017, i.e. approximately two months and a half after the
173 event. We verified that no wave event had occurred in these two intervals. In addition, we
174 checked the relative stability of the shoreline during fair weather periods, using the June 2015
175 and October 2016 images (see SM1). These checks confirmed that available images could be
176 used to assess the impacts of tropical low 13F. The resolution of the images (0.5 m) and
177 image quality were satisfactory for shoreline change digitisation. In addition, the UAV
178 images taken on 10 March 2018 were assembled into an orthomosaic and georeferenced in
179 ArcGIS 10.5.1 using ground control points extracted from the April 2017 Pléiades satellite
180 image.

Date	Sensor	Type	Pixel size
11/06/2015	Pléiades-1B	Multispectral	2 m
11/06/2015	Pléiades-1B	Panchromatic	0.5 m
23/10/2016	Pléiades-1A	Multispectral	2 m
23/10/2016	Pléiades-1A	Panchromatic	0.5 m
29/04/2017	Pléiades-1B	Multispectral	2 m
29/04/2017	Pléiades-1B	Panchromatic	0.5 m

10/03/2018	UAV	RGB image	0.045 m

Table 1. Characteristics of the images used in this study.

Sediment deposits and vegetation density analysis

The analysis of sediment deposits and of the coastal vegetation density required the generation of pan-sharpening images. These images were generated using the Gram Schmidt Pan-sharpening algorithm (Laben and Brower, 2000) and ENVI 5.4 software. They have a spatial resolution of 0.5 m, and were obtained by the fusion of the multispectral images at 2 m resolution with the panchromatic image at 0.5 m. Because the 2015 and 2016 pan-sharpening images had offsets with the 2017 pan-sharpening image, registration was made in ArcGIS 10.5.1 by translation, using geomorphic features as ground control points (2015 translation: X= –1.5 m, Y = –5 m; 2016 translation: X= –2.5 m, Y = –0.5 m).

3.2.2. Image analysis

Shoreline change assessment

We divided the study ocean-facing shoreline into three shoreline sections from west to east, numbered 1, 2 and 3 (Fig. 2b). Shoreline section 1 was divided into sub-sections to account for the alternation of ocean-facing shoreline (1a, 1c, 1e, 1g and 1i) and hoa-type shoreline (1b, 1d, 1f and 1h) (Fig. 3). This was not done for shoreline sections 2 and 3 which only include ocean-facing shoreline. In line with previous studies assessing the impact of storm events on shoreline position (Ford and Kench, 2014, 2016; Duvat et al., 2017a, 2017b), we used the vegetation line as a shoreline proxy (Fig. 4). Along some shoreline sections, especially in the vicinity of hoa, a low-density vegetation cover generally occurs that extends seaward over great distances. In such configurations, we excluded the area covered with scattered plants from the island boundary, considering the continuous vegetated part of islands to correspond to their stable area (Fig. 4c). In addition, digitising the vegetation line was made impossible (i.e. no data areas) by vegetation removal in some areas, especially along the airstrip (Fig. 2b)

and in a quarry area (Fig. 3). To ensure data consistency and quality, the vegetation line was digitised by a single operator and at a fixed and adequate scale of 1:800 (Holdaway and Ford, 2019). Using a second and complementary shoreline indicator to the vegetation line, i.e. the base of the beach, was made impossible as the latter was not detectable due to extensive sediment spreading in the intertidal area.

The errors generated by the three sources of uncertainty to be considered when interpreting shoreline change from satellite imagery – image resolution (pixel size), image georeferencing and shoreline digitization (Ford, 2012, 2013; Yates et al., 2013) – were estimated to be 0.5 m, 0.35 m (due to the residual error resulting from the initial offset between the April 2017 image and other images), and <2 m for the digitisation of the vegetation line. The total vegetation line position error was therefore estimated to be ≤2.85 m. Shoreline change was calculated using the Digital Shoreline Analysis System (DSAS) (Thieler et al., 2009), based on the generation of 10 m interval transects from the baseline. The Net Shoreline Movement (NSM), measuring the distance between two distinct shorelines, was automatically generated for all time series (2015-2016, 2016-2017 and 2015-2017) and shoreline sections (1a-1i, 2 and 3). Transects showing changes ≤– 2.85 m and ≥+ 2.85 m respectively indicate a retreat and an advance of the vegetation line.

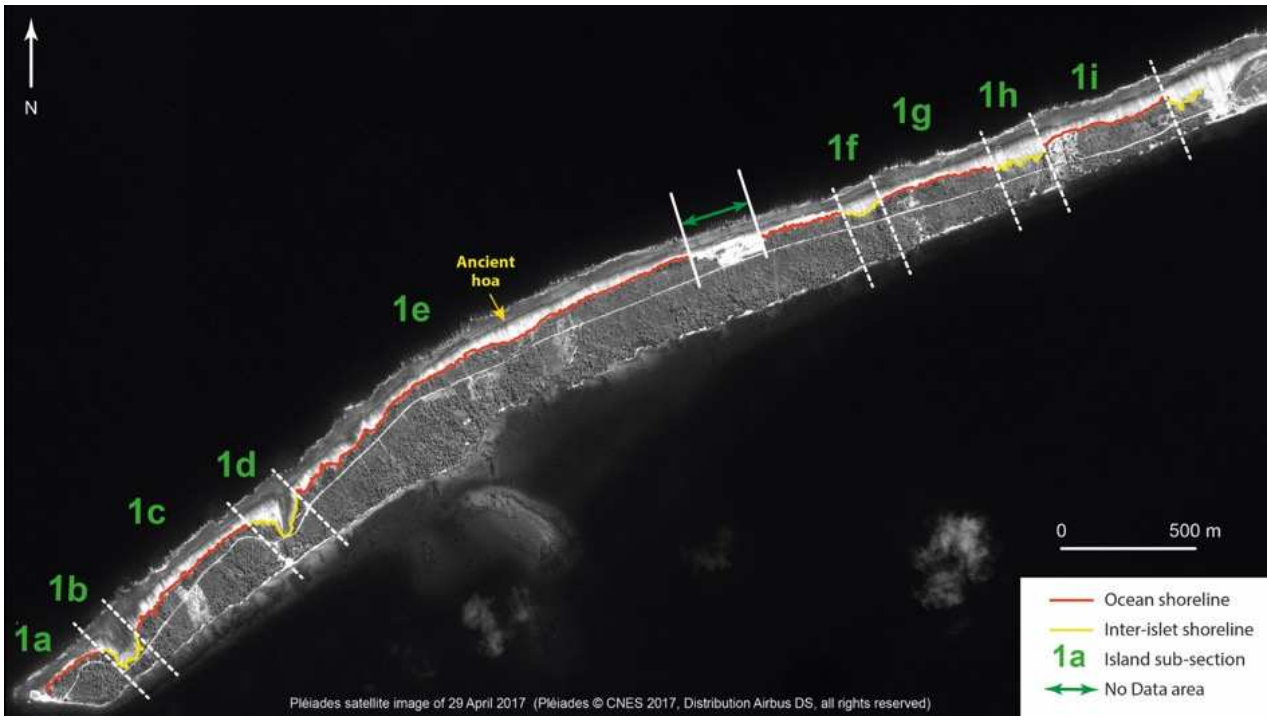

Figure 3. Subdivision of island section 1.

This map shows the subdivisions used to generate shoreline change results, and the differentiation between ocean-facing (in red) and hoa-facing (in yellow) shoreline. The no data area corresponds to a quarry area.

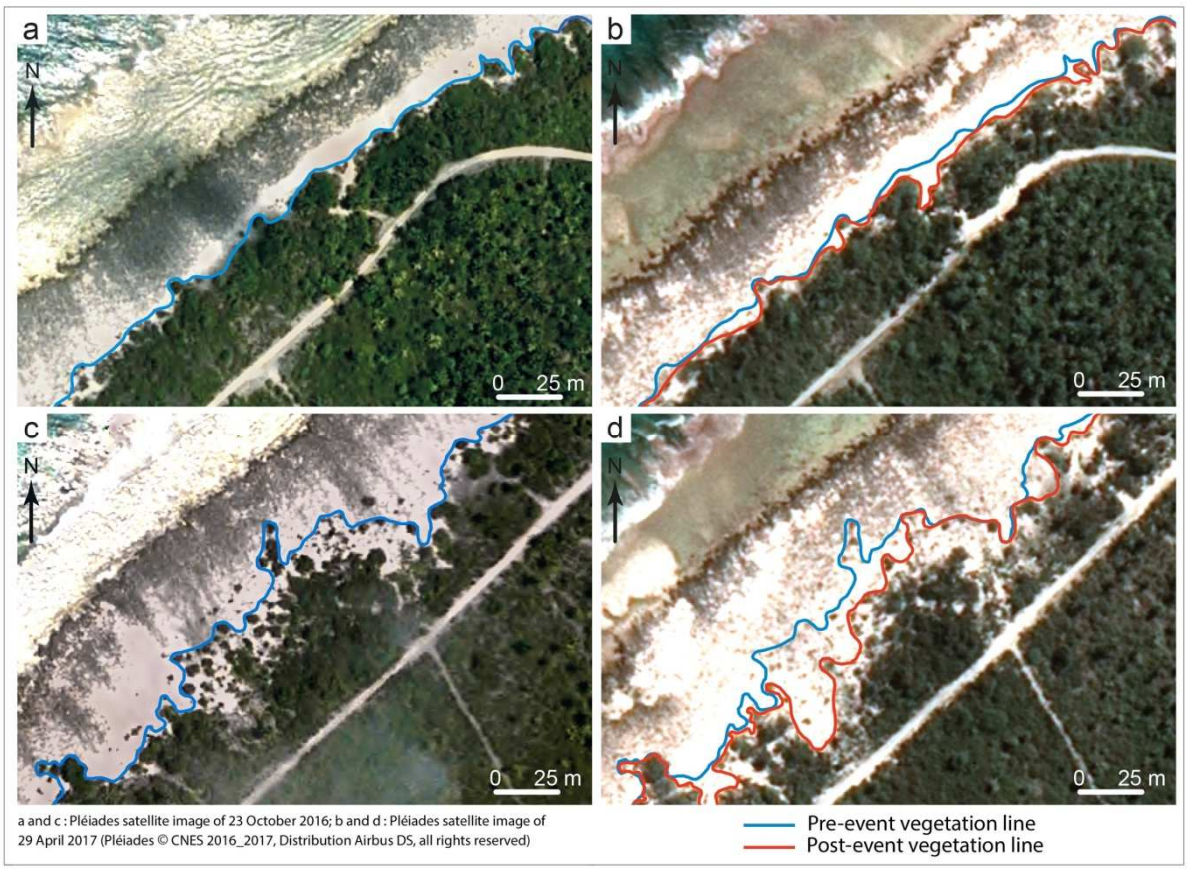

Figure 4. Shoreline indicator used in this study.

We used the vegetation line as a shoreline proxy, and excluded scattered vegetation. a and c illustrate the digitisation of the pre-storm vegetation line in high- and low-density areas, respectively. b and d show the position of the pre- and post-storm vegetation line in the same areas as a and c.

Analysis of storm-generated sediment deposits

The assessment of storm-induced sediment deposits involved (i) field observations, to describe and geolocate sediment deposits, including those located under the vegetation cover; (ii) the comparative analysis of the April 2017 (i.e. post-storm) image and the March 2018 (+ ~11 months) UAV orthomosaic, to analyse changes in the configuration (i.e. shape and area) and position (i.e. migration) of storm ramparts (see SM2 for details); and (iii) classification methods performed on pan-sharpening images using ENVI software, to map changes in the extent of sediment deposits over the period covered by the images. The methodological approach (see SM4) involves Principal Component Analysis (Byrne *and al.*, 1980; Richards, 1999; Chuvieco, 2016) and multistage unsupervised K-means classifications (Tou and Gonzalez, 1974; Jain, 2010).

Vegetation analysis

The Normalised Difference Vegetation Index (NDVI) was applied to the pan-sharpening images to assess coastal vegetation density within a 100 m-wide coastal strip extending landward from the vegetation line. The values obtained are theoretically comprised between –1 and +1, with the negative values corresponding to surfaces other than vegetation cover, such as water or clouds, for which the reflectance in the red is greater than that of the near infrared. While for bare soils the NDVI has values close to 0 (because the reflectances have the same order in the red and the near infrared), the vegetation formations have positive values of

NDVI, generally comprised between 0.1 and 0.7, and increasing with vegetation density (Tucker, 1979).

4. Results

4.1. Storm wave-induced shoreline change

The impact of storm waves on shoreline position decreased eastward, from the highly-exposed islands located immediately to the east of Garuae Pass to the sheltered village area. Shoreline section 1, which was the most exposed to wave action due to its location and to its SW-NE orientation, predominantly exhibited shoreline retreat, which was detected along 54.14% of transects, and secondarily exhibited shoreline stability, noted along 45.86% of transects. Shoreline retreat was marked in its central part (corresponding to sub-sections 1e, 1f and 1g), where 51.11 to 93.33% of transects exhibited retreat (Table 2 and SM3) and where the lowest average and minimum NSM values were respectively comprised between –12.78 m (1f) and –45.46 m (1e). In contrast, the western part (sub-sections 1a, 1b, 1c and 1d) and eastern end (1h) of shoreline section 1 predominantly showed shoreline stability, which was detected along 55.00 (1d) to 85.19% (1a) of transects. In general, hoa shoreline sections did not exhibit higher retreat values compared to ocean-facing shoreline sections. Shoreline sections 2 and 3 predominantly experienced stability, which was detected along 62.72% and 97.65% of transects, respectively. Along shoreline section 2, 36.56% of transects showed retreat.

Beyond general trends, i.e. the prevalence of retreat and stability, respectively, along shoreline sections 1 and 2, these two shoreline sections showed high alongshore variability in shoreline response, with some transects exhibiting a marked retreat while others (sometimes nearby transects) exhibited stability (Table 2). The lowest NSM values obtained were <–17 m for 6 out of the 9 sub-sections of shoreline section 1 and of –26.13 m for shoreline section 2.

The almost absence of erosional transects along shoreline section 3 reflects its sheltered position in relation to the storm waves. These results reflect the significant impact of these storm waves on the exposed, i.e. north-facing, ocean coast of the atoll.

Sub-sections	Number of transects	Mean NSM (m)	Min. NSM (m)	Max. NSM (m)	Accretional transects		Stable transects		Erosional transects	
					Nb	%	Nb	%	Nb	%
1a	27	-1.31	-7.09	0.00	0	0.00	23	85.19	4	14.81
1b*	13	-2.19	-9.19	0.17	0	0.00	10	76.92	3	23.08
1c	59	-3.35	-19.76	0.09	0	0.00	37	62.71	22	37.29
1d*	20	-4.79	-30.77	0.00	0	0.00	11	55.00	9	45.00
1e	210	-6.36	-45.46	2.75	0	0.00	70	33.33	140	66.67
1f*	15	-12.78	-33.91	-2.43	0	0.00	1	6.67	14	93.33
1g	45	-3.70	-14.08	0.00	0	0.00	22	48.89	23	51.11
1h*	32	-4.74	-31.21	0.00	0	0.00	21	65.63	11	34.37
1i	50	-5.37	-17.03	0.03	0	0.00	21	42.00	29	58.00
Total 1a-1i	471	/	/	/	0	0.00	216	45.86	255	54.14
2	279	-3.01	-26.13	4.13	2	0.72	175	62.72	102	36.56
3	339	0.56	-3.64	3.93	7	2.06	331	97.65	1	0.29

Table 2 – Changes in the position of the vegetation line on ocean and inter-islet channel shores over the 2015-2017 period. *sub-sections correspond to inter-islet shoreline.

4.2. The predominance of constructional vs. erosional impacts

Tropical low 13F caused extensive sediment injection into the intertidal area, that is, on the conglomerate platform (Figs. 5 and 6), as a result of the *(i)* mechanical destruction on the outer slopes (confirmed by the diving instructors interviewed) and transfer to the conglomerate platform of living corals (Fig. 6c), *(ii)* transfer of loose material, especially sand and smooth and rounded coral rubble and blocks from the spur and groove reservoir to the conglomerate platform (Figs. 6a, 6b, 8), and *(iii)* dismantling of the conglomerate platform,

294 which provided sand and smooth and rounded coral rubble and blocks that were transferred to
295 the coast (Fig. 6d). Extensive sand and rubble sheets and tracts formed (Figs. 5 and 6a, 6b),
296 stretching from the seaward boundary of the conglomerate platform where no sediment
297 accumulation was present before the event to the coast and even to interior areas, especially
298 where shore-perpendicular tracks facilitated wave penetration (Fig. 5a). Although this was not
299 measurable, in March 2018, we noted significant landward transfer of the sediment that had
300 initially accumulated on the seaward edge of the conglomerate platform. Additionally, this
301 storm event reactivated some non-functional hoa (Figs. 5b, 5c). Moreover, massive sand and
302 rubble accumulation occurred on the east-west track connecting islands between Garuae Pass
303 and Rotoava, which reached up to 100 m landward from the vegetation line.

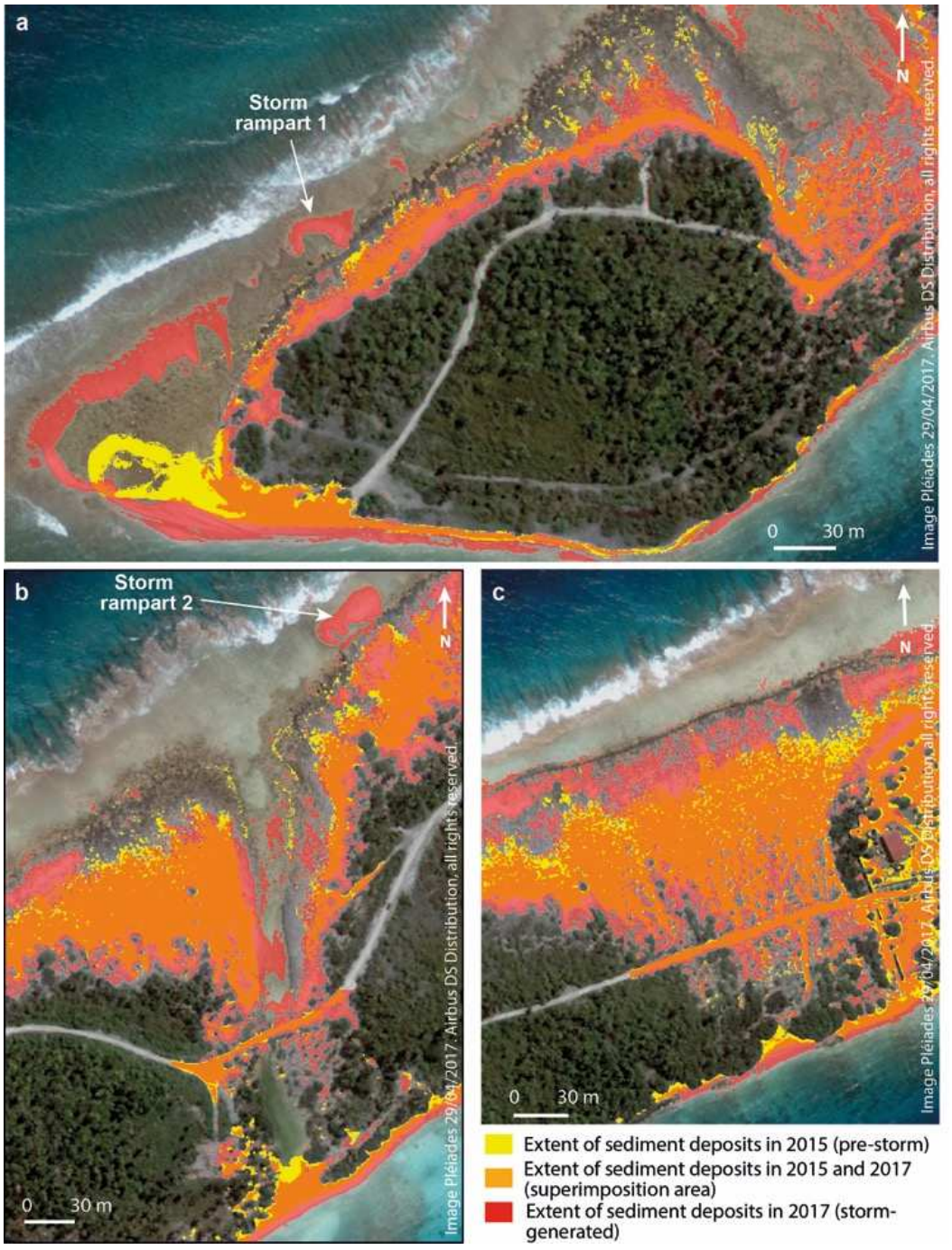

Figure 5. Mapping of pre-storm and post-storm sediment deposits, including superimposition areas.

These maps highlight (in red) the extent of storm-generated sediment deposits in intertidal (including sediment sheets and tracts and the formation of two storm ramparts), coastal and inland areas. a shows massive sediment injection from the spur and groove system onto the narrow (~50 m here) conglomerate platform nearby Garuae Pass. b and c illustrate the injection of sediments on the outer, i.e. seaward, border of the conglomerate platform

311 that showed no sediment accumulation before the event; they also emphasise ocean-to-island sediment transfer
312 through hoa (b) and in ancient hoa (c)

313

314 Figure 6. Accretional impacts of tropical low 13F.

315 a and b show sediment sheets. c illustrate living coral inputs from the spur and groove reservoir. d show
316 important sediment inputs in a non-vegetated area and induced sediment accumulation on the main track that
317 connects western islands to the village.

318

319 Importantly, this event led to the formation of two small storm ramparts on the seaward edge
320 of the conglomerate platform (Figs. 7 and 8) in shoreline section 1 (i.e. the most exposed to
321 the storm waves). These ramparts respectively formed at a distance of ~83 m (R1) and
322 ~1.3 km (R2) from Garuae Pass (see location in Fig. 2). At the time of their formation, R1 and
323 R2 respectively measured 30 and 41 m in their longest axis, had maximum heights of ~1.30 m
324 and ~2.0 m, and a surface area of ~229.52 m^2 and ~593.08 m^2. They were principally
325 composed of small coral debris (5-10 cm in diameter), mixed up with coral blocks measuring
326 30 to 50 cm in diameter. The material composing these two ramparts was a mix of fresh
327 corals and loose (and smooth) rubble. After one year, these two ramparts had undergone
328 major changes in configuration and position. Both showed important sediment reworking and
329 landward migration. In March 2018, R1 had considerably lengthened (from 30 to 80 m in its
330 longest axis, area of 412.96 m^2), while its centre of gravity had moved landward by 23.1 m. In
331 the same time, R2 underwent more limited changes in shape and position, as its length
332 increased from 41 to 48 m (area of 599.95 m^2) while its landward migration was limited to
333 10.7 m.

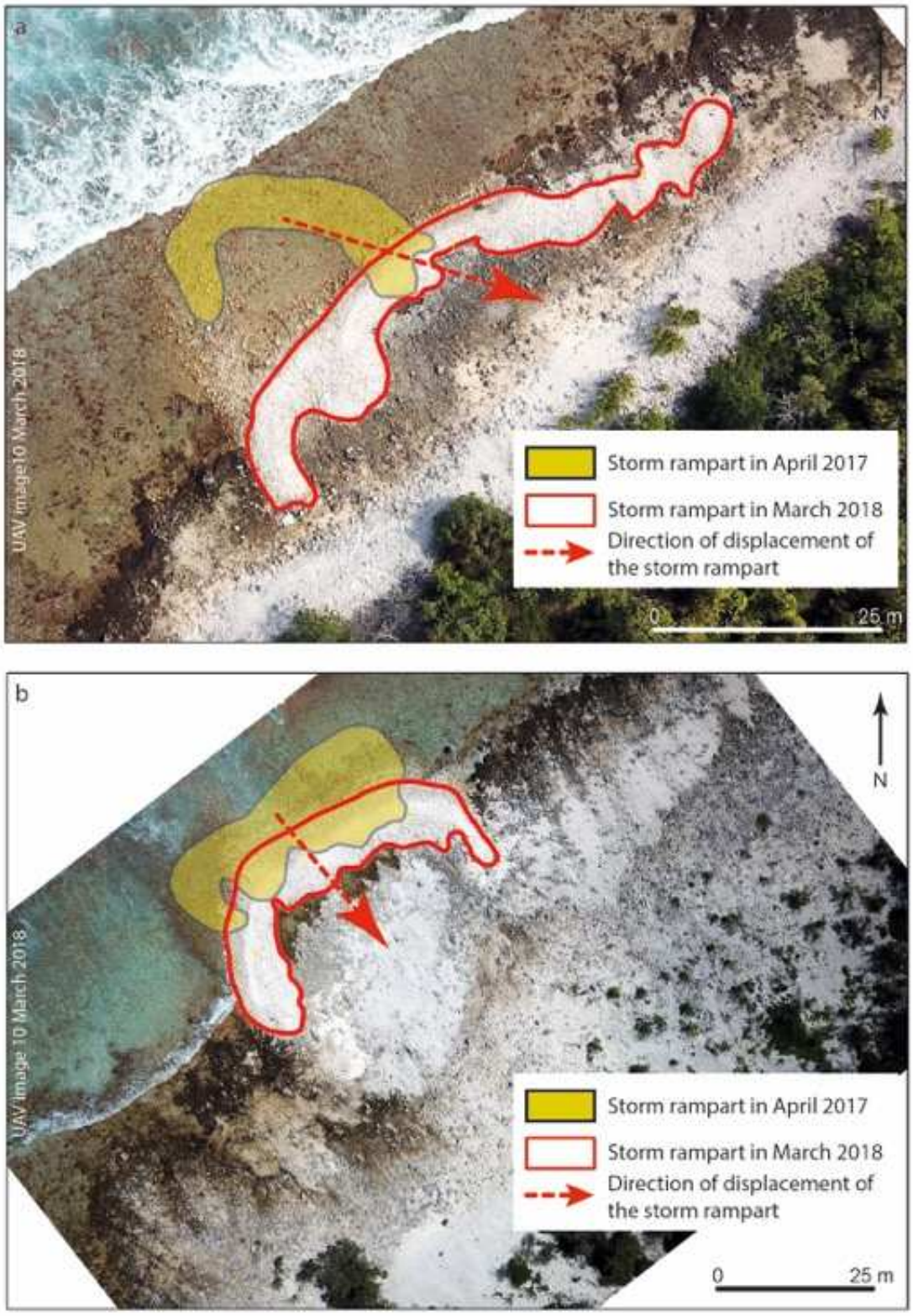

334

335 Figure 7. Changes in the configuration and position of the storm ramparts after one year.

336 a shows R1, which formed at a distance of ~83 m from Garuae Pass and underwent marked changes in shape and

337 position. b shows R2, which was more massive and underwent limited changes in configuration and position,

338 despite, like R1, a significant landward migration.

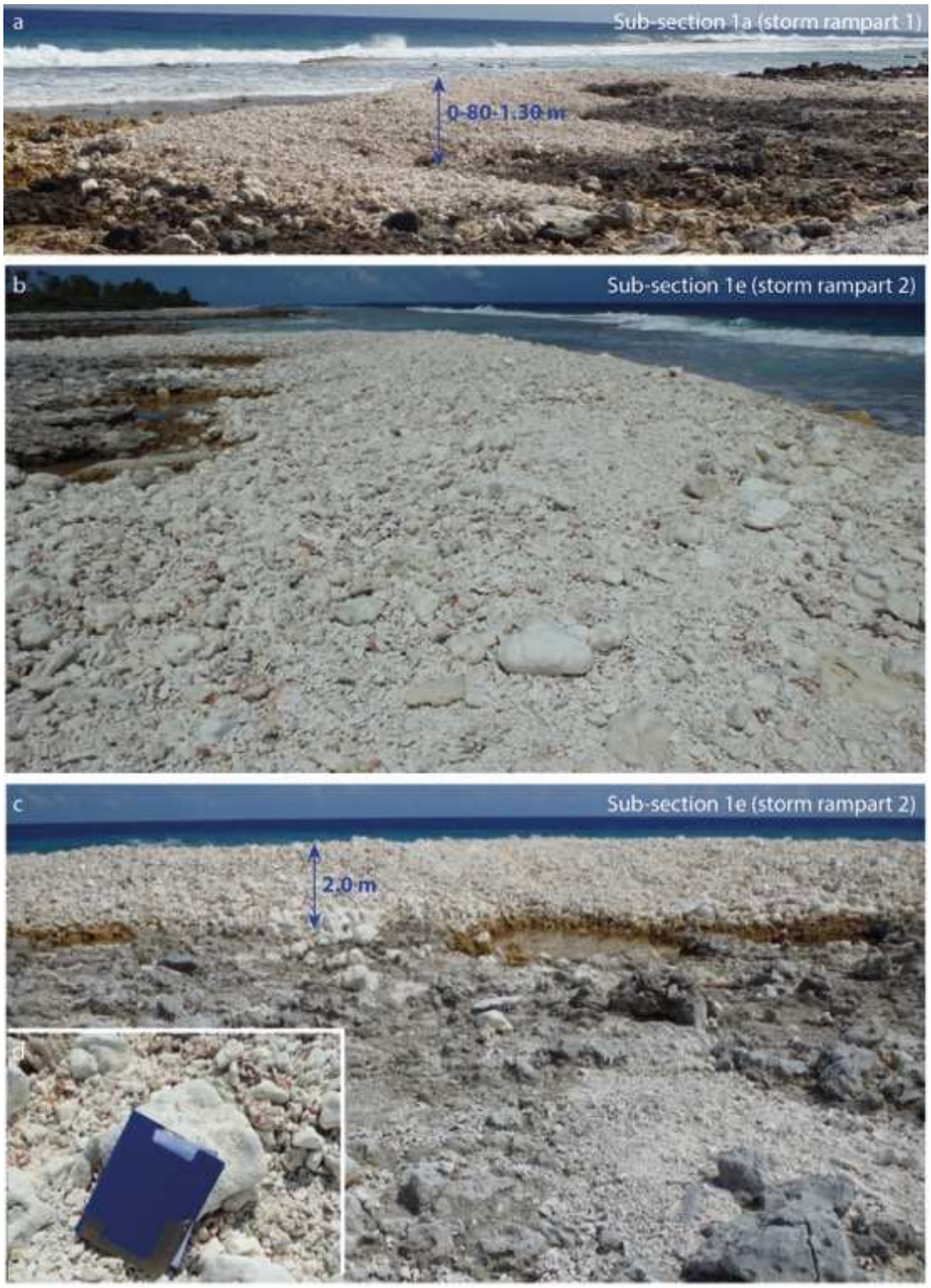

339

340 Figure 8. Storm ramparts one year after their formation (March 2018).

341 a shows the longitudinal profile of R1, while b and c illustrate the more massive character of R2. d shows the

342 material composing R2.

343

344 Tropical low 13F also caused marked erosion, including in the intertidal area, where the
345 waves caused the dismantling and scouring of the conglomerate platform, both in its outer
346 (Fig. 9a) and inner (Fig. 9b) parts, and in the coastal area, where wave attack caused not only
347 the retreat of the vegetation line, but also localised soil scouring. However, on the whole, the
348 areas experiencing sediment deposition predominated.

349

350 Figure 9. Erosional impacts of tropical low 13F on the conglomerate platform.

a illustrates the contribution of storm waves to the dismantling of the outer part of the conglomerate platform and transfer of the smooth coral rubble and blocks removed from this platform to the shore. b shows that the dismantling and scouring of this platform also occurred in its inner part, where it connects to the base of the beach.

4.3. Interferences of human activities with storm-driven processes

In the study area, the major mode of interference of human activities with storm-driven processes relates to the degradation, i.e. either partial or total destruction, depending on locations, of the coastal vegetation belt composed of native species, which exacerbated wave incursion inland. This was observed first, in the airstrip area (see location in Fig. 2a), where the removal of the vegetation on both sides of the airstrip for security purposes allowed the waves to cross over the island from ocean to lagoon, which caused extensive sediment deposition on the airstrip (Fig. 10a). The same phenomenon, i.e. extensive overwash causing massive sediment deposition, occurred in the quarry area (see location in Fig. 2a), where the nearly total destruction of the coastal vegetation over a 70 m-wide and 300 m-long area generated massive sediment accumulation, including on the west-east track and in the vegetated area extending landward from this track (Fig. 10b). The waves also penetrated far inland in the axis of the shore-perpendicular tracks connecting the ocean-side beaches to the west-east track (Fig. 10c). In most depositional areas, sediment deposits, which consisted of sand, coral debris and blocks, were a few centimetres thick. However, we also observed sediment deposits reaching up to a few decimetres in thickness, especially in the extension of hoa, on the west-east track and on some shore-perpendicular tracks.

374

375 Figure 10. Interferences of human activities with storm-driven processes.

376 a illustrates the impacts of the storm waves on the airstrip, i.e. extensive sediment deposition resulting from the
377 removal of the coastal vegetation. b shows the exacerbation of overwash processes and associated sediment
378 deposition in the quarry area, where the coastal vegetation has been extensively removed. c illustrates extensive
379 wave incursion inland in the axis of shore-perpendicular tracks.

380

381 Furthermore, Net Shoreline Movement (NSM, i.e. distance between the pre- and post-storm
382 vegetation line position) values are generally (although not systematically) in accordance with
383 NDVI values indicating pre-storm vegetation density (Figs. 11). The highest NSM values (i.e.
384 comprised between 0 and –5 m and indicating limited shoreline retreat) correspond to the
385 highest (i.e. reaching up to 0.56) NDVI values indicating high vegetation density (Fig. 12).
386 Conversely, the lowest NSM values (comprised between –25 and –45 m and indicating
387 marked shoreline retreat) correspond to the lowest (i.e. <0.35) NDVI values indicating low
388 vegetation density. These findings indicate that a dense coastal vegetation belt composed of
389 native species is more resistant to storm waves than a low-density vegetation cover. We also
390 observed that where the coastal vegetation belt was dense, soil scouring was limited and
391 sediment deposition was important and restricted to a 10-to-20 m wide coastal strip. This
392 confirms the major role of a healthy coastal vegetation belt in protecting soils from storm-
393 induced scouring and in promoting beach ridge building.
394

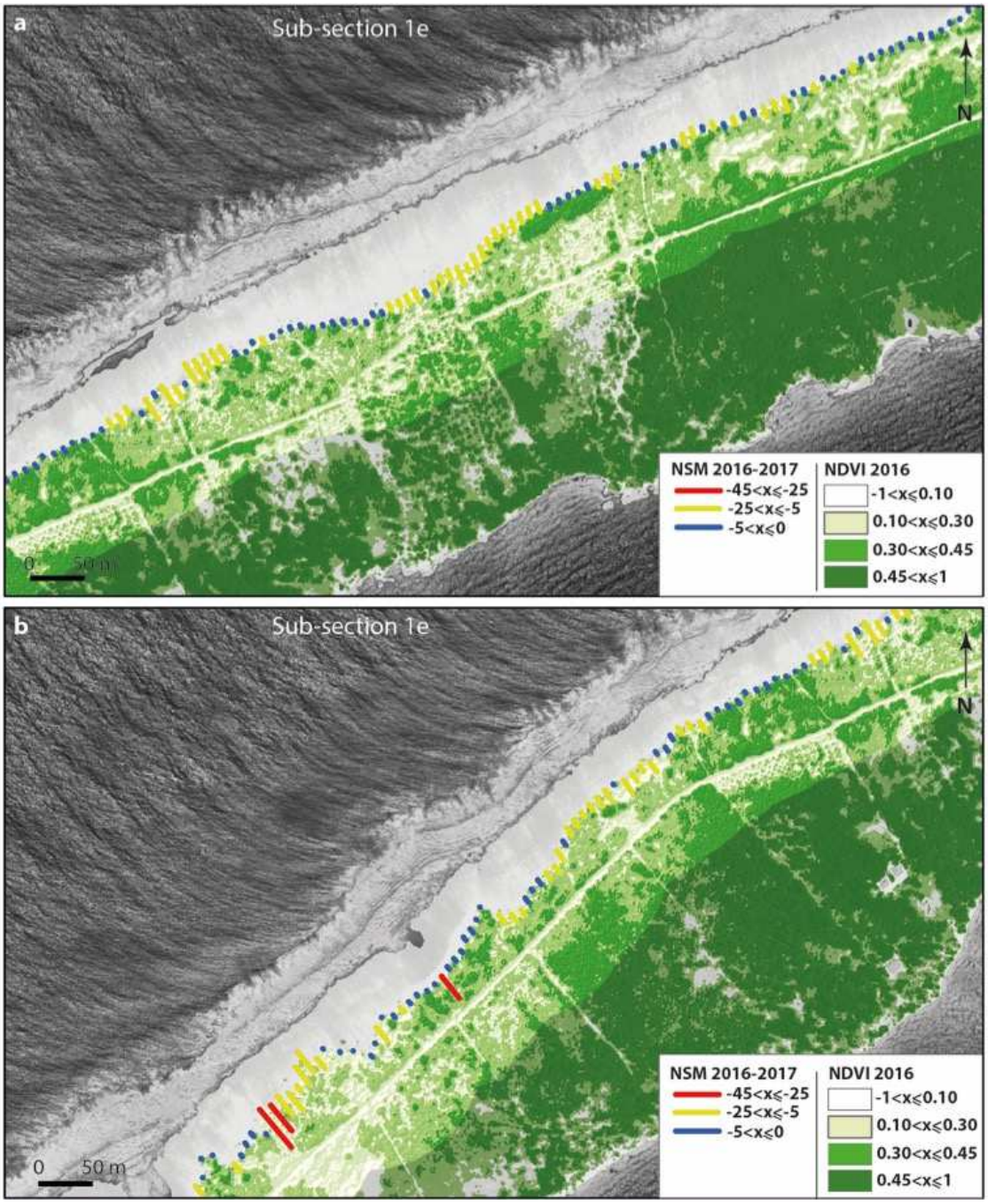

395

396 Figure 11. Relationship between shoreline response and coastal vegetation density.

397 a and b show that Net Shoreline Movement (NSM) values, which reflect shoreline response, are the smaller

398 where coastal vegetation density (reflected by 0.10 to 1 NDVI values) are the highest and vice versa.

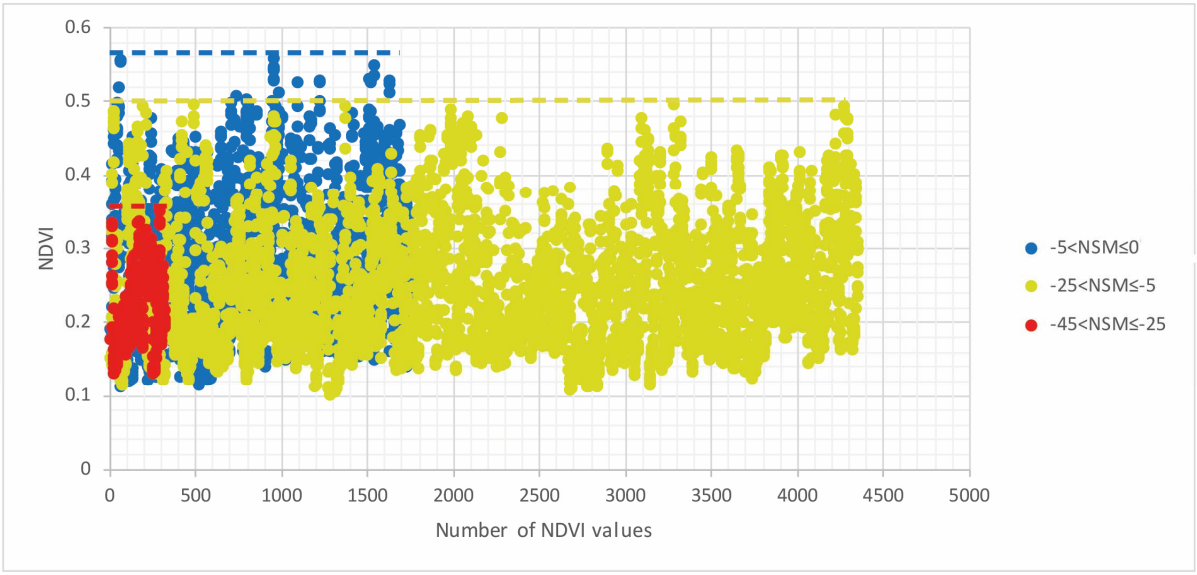

399
400 Figure 12. Distribution of NDVI values according to NSM values.

401 The highest NSM values (i.e. comprised between 0 and –5 m and indicating limited shoreline retreat)
402 correspond to the highest (i.e. reaching up to 0.56) NDVI values indicating high vegetation density
403 (Fig. 12). Conversely, the lowest NSM values (comprised between –25 and –45 m and indicating
404 marked shoreline retreat) correspond to the lowest (i.e. <0.35) NDVI values indicating low vegetation
405 density.

406

407

5. Discussion

5.1. Implications for future research

Moderate climate events such as tropical low 13F have so far been overlooked by geomorphic studies on atolls, which have focused on the impacts of more spectacular, i.e. high-energy, climate events, such as tropical cyclones and strong distant-source swells. This study is the first one that investigates the geomorphic impacts of a moderate climate event. Importantly, our findings show that such climate events, which are much more frequent than tropical cyclones – to be precise have a return period of ~ 2-3 years against 39 years for tropical cyclones in the northwestern Tuamotu atolls – have unexpected and significant geomorphic impacts on atoll islands. The waves generated by tropical low 13F had marked impacts all along the north-facing exposed ocean coast of the atoll. However, in the study area, the vegetation line predominantly exhibited stability, which was detected along 52.13% of transects, while retreat was observed along 47.60% of transects. This finding, together with the large extent of constructional features, including sand and rubble sheets and tracts and two small storm ramparts that all showed significant landward migration after one year, highlights that such moderate storms mainly have constructional effects. In this case, the storm waves injected massive sediment inputs into the island system through the mechanical destruction of living corals on the outer slopes and the transfer of loose and smooth coral rubble and blocks from the spur and groove reservoir (where these materials had accumulated) and conglomerate platform, which suffered marked dismantling, to the beaches and even to inland areas. At several locations, the storm waves even crossed over the islands, reaching the lagoon. Such extensive impacts, both erosional and accretional, were so far known to be generated by high-energy climate events such as tropical cyclones and distant-source swells. This study therefore brings new insights on atoll island change by demonstrating the

significant contribution, and especially the accretional impact, of a moderate climate event to island and shoreline change.

Based on these observations, we advocate that extensively assessing the geomorphic impacts of such events on atoll islands is urgently needed to improve the understanding of atoll island dynamics. Such knowledge is crucial in the current climate change context, in which climate-related pressures are rapidly increasing in atoll regions and are expected to cause increased shoreline retreat and island destabilisation (Beetham et al., 2017; Shope and Storlazzi, 2019; Tuck et al., 2019). In fact, determining whether relatively frequent moderate climate events – i.e. not only tropical lows forming in the intertropical zone, but also moderate distant-source swells that affect the northwestern Tuamotu atolls 2 to 3 times a year according to their inhabitants – offset the sediment losses caused by extreme climate events seems crucial to properly understand atoll island change. In those atoll regions where tropical cyclones are uncommon (e.g. in the Tuamotu Archipelago, Larrue and Chirron, 2010; in the Marshall Islands, Ford and Kench, 2014, 2016; in the Maldives, Aslam and Kench, 2017), moderate climate events probably play a more determinant role in island dynamics and change than extreme climate events. Consequently, increased research efforts are needed on both their frequency (not only current, but also projected) and their effects on atoll islands.

5.2. Implications for risk reduction on atolls

Our findings also provide major insights for coastal risk reduction on atolls. Given that the impacts of moderate climate events, including overwash and extensive sediment deposition, are significant and may reach the interior of islands, especially in low-lying and non-vegetated areas, it seems crucial to preserve the coastal vegetation belt which buffers storm waves and protects inner areas from their devastating effects from human-induced destruction. The spatial correlations between (i) vegetation density (i.e. condition) and

457 shoreline response – with shoreline retreat being inversely proportional to vegetation density
458 –, and (ii) vegetation density and the extent of overwash-induced sediment deposition,
459 advocates for the preservation, and even for the restoration where it has been destroyed, of the
460 coastal vegetation belt. Removing the coastal vegetation exacerbates shoreline retreat, soil
461 scouring, while also increasing the extent of overwash and of inland sediment deposition.
462 Such an exacerbation of storm impacts on both shoreline and island, which was not really
463 problematic (except on the airstrip) in the present case, would have much more serious
464 consequences in a densely-settled area. Where atoll reef-island systems keep exhibiting
465 natural accretional processes, as the ones described in this study, nature-based solutions,
466 which describe 'actions to protect, sustainably manage, and restore natural or modified
467 ecosystems that address societal challenges (e.g. climate change, food and water security or
468 natural disasters) effectively and adaptively, while simultaneously providing human well-
469 being and biodiversity benefits' (Cohen-Shacham et al., 2016: 2), should be prioritised. The
470 same conclusion arose from previous studies addressing tropical cyclone impacts, which also
471 highlighted not only the constructional impacts of such events, but also the exacerbation of
472 coastal erosion and flooding where human activities had led to the entire or partial destruction
473 of the coastal vegetation belt (Stoddart, 1963, 1965; Duvat et al., 2017a).
474
475 **6. Conclusions**
476 The study of the impacts of a moderate climate event, i.e. tropical low 13F, on Fakarava
477 Atoll, in the northwestern Tuamotu Archipelago, French Polynesia, based on field
478 observations and multi-date image analysis, brings important new insights to the
479 understanding of atoll island dynamics. Importantly, it shows that such events, which are
480 much more frequent than tropical cyclones (return period of 2-3 years against 39 years in the
481 present case), and have so far been overlooked, (1) have significant geomorphic impacts on

atoll islands, and even comparable impacts (at least in nature, e.g. causing shoreline retreat and the formation of storm ramparts and extensive sediment sheets and tracts on the reef flat) to those of intense tropical cyclones, (2) contribute to island building through the injection of massive sediment inputs into the island system, due both to the mechanical destruction of living corals on the outer slopes and the transfer to the intertidal, coastal and inland areas, of loose sediments that had accumulated in the spur and groove area and on the conglomerate platform, (3) have less extensive (i.e. restricted to the intertidal and coastal zones) impacts where the coastal vegetation belt composed of native species has been preserved, while reaching inland areas over great distances (>100 m here) where the latter has been destroyed. This last finding advocates for the promotion of nature-based solutions to face coastal erosion and flooding in such settings, that is, for the preservation or restoration of the coastal vegetation, and beyond, for the recognition that a continuum of healthy ecosystems (i.e. from the reef ecosystem to inland areas, including the coastal vegetation) is required to maintain coastal risks as low as possible on atoll islands.

In addition, these findings call for the more systematic assessment of the impacts of moderate climate events, as these events, which include not only tropical lows that form in the intertropical zone but also moderate distant-source swells, are much more frequent than tropical cyclones, especially (but not only) in atolls areas that are located outside the cyclone belt such as the Central Pacific (Tuamotu region), the Western (Marshall Islands) and equatorial Pacific, and the central Indian Ocean (Maldives Islands). For example, in the Western Tuamotu that are the subject of this study, tropical cyclones have a return period of ~39 years, while tropical lows and moderate distant-source swells respectively occur every 2-3 years and 2-3 times a year. This study thus reveals an important research gap in atoll geomorphic studies, which requires increased scientific efforts in the future, as such constructional events may, at least in some atoll contexts (i.e. where tropical cyclones are

uncommon) offset the potentially erosive (at least at some locations) impacts of increasingly frequent extreme climate events.

Acknowledgements

This work was supported by the French National Research Agency under the STORISK research project (No. ANR-15-CE03-0003). The authors warmly thank the municipality and the inhabitants of Fakarava for providing highly valuable information during the conduction of this study.

References

Andrefouët, A., Ardhuin, F., Queffeulou, P., Legendre, R., 2012. Island shadow effects and the wave climate of the Western Tuamotu Archipelago (French Polynesia) inferred from altimetry and numerical model data. Mar. Pollut. Bull. 65: 415-424. http://dx.doi.org/10.1016/j.marpolbul.2012.05.042.

Aslam, M., Kench, P.S., 2017. Reef island dynamics and mechanisms of change in Huvadhoo Atoll, Republic of the Maldives, Indian Ocean. Anthropocene 18: 57-68. http://dx.doi.org/10.1016/j.ancene.2017.05.003.

Baines, G. B.K., Beveridge, P.J., Maragos, J.E., 1974. Storms and island building at Funafuti Atoll, Ellice Islands, Proc. 2nd Intern. Coral Reef Symp., Vol. 2: 485-496.

Baines, G. B.K., McLean, R. F., 1976. Sequential studies of hurricane deposit evolution at Funafuti Atoll. Mar. Geol. 21: 1–8. http://dx.doi.org/10.1016/0025-3227(76)90097-9.

Becker, M., Meyssignac, B., Letetrel, C., Llovel, W., Cazenave, A., Delcroix, T., 2012. Sea level variations at tropical Pacific islands since 1950. Glob. Planet. Chang. 80–81: 85–98. http://dx.doi.org/10.1016/j.gloplacha.2011.09.004.

532 Beetham, E., Kench, P. S., Popinet, S., 2017. Future Reef Growth Can Mitigate Physical Impacts of
533 Sea-Level Rise on Atoll Islands, Earth's Future 5, 1002–1014.
534 http://dx.doi.org/10.1002/2017EF000589.
535 Byrne, G. F., Crapper, P. F., Mayo, K. K. 1980. Monitoring land-cover change by Principal
536 Component Analysis of multitemporal data. Remote Sens. Environ. 10, 175–184.
537 https://doi.org/10.1016/0034-4257(80)90021-8
538 Canavesio, R., 2019. Distant swells and their impacts on atolls and tropical coastlines. The example of
539 submersions produced by lagoon water filling and flushing currents in French Polynesia during
540 1996 and 2011 mega swells. Glob. Planet. Chang. 177, 116-126.
541 http://dx.doi.org/10.1016/gloplacha.2019.03.018.
542 Church, J.A., White, N.J., 2011. Sea-level rise from the late 19th to the early 21st century. Surv.
543 Geophys. 32:585–602. http://dx.doi.org/10.1007/s10712-011-9119-1.
544 Chuvieco, E., 2016. Fundamentals of Satellite Remote Sensing: An Environmental Approach. 2nd ed.
545 CRC Press. ISBN : 9781498728058
546 Cohen-Shacham, E., Walters, G., Janzen, C., Maginnis, S. (eds.), 2016. Nature-based Solutions to
547 address global societal challenges. Gland, Switzerland: IUCN. xiii + 97pp.
548 Duvat, V., Pillet, V., 2017. Shoreline changes in reef islands of the Central Pacific: Takapoto Atoll,
549 Northern Tuamotu, French Polynesia. Geomorphology 282:96–118.
550 https://dx.doi.org/10.1016/j.geomorph.2017.01.002.
551 Duvat, V.K.E., Volto, N., Salmon, C., 2017a. Impacts of category 5 tropical cyclone Fantala (April
552 2016) on Farquhar Atoll, Seychelles Islands, Indian Ocean. Geomorphology 298: 41-62.
553 http://dx.doi.org/10.1016/j.geomorph.2017.09.022.
554 Duvat, V.K.E., Salvat, B., Salmon, C., 2017b. Drivers of shoreline change in atoll reef islands of the
555 Tuamotu Archipelago, French Polynesia. Glob. Planet. Chang. 158: 134-154.
556 http://dx.doi.org/10.1016/j.gloplacha.2017.09.016.
557 Duvat, V.K.E., Magnan, A.K.M., Canavesio, R., 2018. La reconstruction de chaînes d'impacts au
558 service de l'évaluation de la résilience des territoires et de la réduction des risques météo-marins :

559 le cas des atolls des Tuamotu, Polynésie française. La Houille Blanche 2, 13-21.
560 https://doi.org/10.1051/lhb/2018016
561 Ford, M., 2012. Shoreline changes on an urban atoll in the central Pacific Ocean:Majuro Atoll,
562 Marshall Islands. J. Coast. Res. 28:11–22. https://doi.org/10.2112/JCOASTRESD-11-00008.1.
563 Ford, M., 2013. Shoreline changes interpreted from multi-temporal aerial photographs and high
564 resolution satellite images: Wotje Atoll, Marshall Islands. Remote Sens. Environ. 135:130–140.
565 https://doi.org/10.1016/j.rse.2013.03.027.
566 Ford, M.R., Kench, P.S., 2014. Formation and adjustment of typhoon-impacted reef islands interpreted
567 from remote imagery: Nadikdik Atoll, Marshall Islands. Geomorphology 214, 216–222.
568 http://dx.doi.org/10.1016/j.geomorph.2014.02.006.
569 Ford, M.R., Kench, P.S., 2016. Spatiotemporal variability of typhoon impacts and relaxation on Jaluit
570 Atoll, Marshall Islands. Geology 44(2), 159-162. http://dx.doi.org/10.1130/G37402.1.
571 Hoeke, R.K., McInnes, K.L., Kruger, J., McNaught, R., Hunter, J., Smithers, S., 2013. Widespread
572 inundation of Pacific islands by distant-source wind-waves. Glob. Environ. Chang. 108: 128-138.
573 http://dx.doi.org/10.1016/j.gloplacha.2013.06.006.
574 Holdaway, A., Ford, M., 2019. Resolution and scale controls on the accuracy of atoll island shorelines
575 interpreted from satellite imagery. Applied Geomatics. http://dx.doi.org/10.1007/s12518-019-
576 00266-7.
577 ISPF (Institut Statistique de la Polynésie française) 2017. Statistical data of French Polynesia.
578 http://www.ispf.pf/
579 Jain, A.K., 2010. Data clustering: 50 years beyond K-means. Pattern Recognition Letters 31(8), 651-
580 666. https://doi.org/ 10.1016/j.patrec.2009.09.011
581 Kench, P.S., McLean, R., Brander, R., Nicholl, S.L., Smithers, S., Ford, M., Parnell, K.E., Aslam, M.,
582 2006. Geological effects of tsunami on mid-ocean atoll islands: the Maldives before and after the
583 Sumatran tsunami. Geology 34(3). http://dx.doi.org/10.1130/G21907.1.
584 Laben C.A., Brower B.V., 2000. Process for enhancing the spatial resolution of multispectral imagery
585 using pan-sharpening. Google Patents.

586 Larrue, S., Chiron, T., 2010. Les îles de Polynésie française face à l'aléa cyclonique. VertigO 10 (3).
587 http://vertigo.revues.org/10558.
588 Laurent, V., Varney, P., 2014. Historique des cyclones de Polynésie Française de 1981 à 2010. Météo-
589 France Direction interrégionale de la Polynésie Française, Etudes et Climatologie, Tahiti, 175 p.
590 Le Cozannet, G., Garcin, M., Petitjean, L., Cazenave, A., Becker, M., Meyssignac, B., Walker, P.,
591 Devilliers, C., Le Brun, O., Lecacheux, S., Baills, A., Bulteau, T., Yates, M., Wöppelmann, G.,
592 2013. Exploring the relation between sea level rise and shoreline erosion using sea level
593 reconstructions: an example in French Polynesia. J. Coast. Res. 65, 2137-2142.
594 https://doi.org/10.2112/SI65-361.1
595 Maragos J. E., Baines G. B. K., Beveridge P. J., 1973. Tropical Cyclone Bebe Creates a New Land
596 Formation on Funafuti Atoll. Science 181 (4105), 1161-1164.
597 http://dx.doi.org/10.1126/science.181.4105.1161.
598 Nurse, L.A., McLean, R.F., Agard, J., Briguglio, L.P., Duvat-Magnan, V., Pelesikoti, N., Tompkins,
599 E., Webb, A., 2014. Small islands. In: Barros, V.R., Field, C.B., Dokken, D.J., Mastrandrea, M.D.,
600 Mach, K.J., Bili, T.E., Chatterjee M., Ebi, K.L., Estrada, Y.O., Genova, R.C., Girma, B., Kissel,
601 E.S., Levy, A.N., MacCracken, S., Mastrandrea, P.R., White, L.L. (Eds.), Climate Change 2014:
602 Impacts, Adaptation and Vulnerability. Part B: Regional Aspects. Contribution of Working Group
603 II to the Fifth Assessment Report of the Intergovernmental Panel on Climate Change. Cambridge
604 University Press, Cambridge and New York, pp.1613–1654.
605 Pirazzoli, P.A., Montaggioni, L.F., 1986. Late Holocene sea-level changes in the northwest Tuamotu
606 islands, French Polynesia. Quaternary Research 25(3), 350-368. http://dx.doi.org/10.1016/0033-
607 5894(86)90006-2.
608 Rankey, E. C., 2011: Nature and stability of atoll island shorelines: Gilbert Island chain, Kiribati,
609 equatorial Pacific. Sedimentology 58 (7), 1831-1859. http://dx.doi.org/10.1111/j.1365-
610 3091.2011.01241.x.
611 Richards, J.A., Jia, X. 2006. Remote Sensing Digital Image Analysis: An Introduction, Springer-
612 Verlag, Berlin Heidelberg, 439 p.

Rougerie, F., 1994. Nature et fonctionnement des atolls des Tuamotu (Polynésie Française). Oceanologica Acta 18(1), 61–78.

Scoffin, T.P., 1993. The geological effects of hurricanes on coral reefs and interpretation of storm deposits. Coral Reefs 12, 203-221. http://dx.doi.org/10.1007/BF00334480.

Shope, J. B., Storlazzi, C. D. 2019. Assessing Morphologic Controls on Atoll Island Alongshore Sediment Transport Gradients Due to Future Sea-Level Rise. Front. Mar. Sci. 6, http://dx.doi.org/10.3389/fmars.2019.00245.

Smithers, S.G., Hoeke, R.K., 2014. Geomorphological impacts of high-latitude storm waves on low-latitude reef islands. Observations of the December 2008 event on Nukutoa, Takuu, Papua New Guinea. Geomorphology 222: 106–121. http://dx.doi.org/10.1016/j.geomorph.2014.03.042.

Stoddart, D.R., 1963. Effects of hurricane Hattie on the British Honduras reefs and cays, October 30–31, 1961. Atoll Res. Bull. 95, 1–142.

Stoddart, D.R., 1965. Re-survey of hurricane effects on the British Honduras reefs and cays. Nature CCVII, pp. 589–592.

Stoddart, D. R., 1969. Post-hurricane changes on the British Honduras reefs and cays: re-survey of 1965. Atoll Research Bulletin, 131, 36 p.

Stoddart, D. R., 1971. Coral reefs and islands and catastrophic storms. In: Steers, J.A. (Ed.), Applied Coastal Geomorphology, Palgrave Macmillan, UK, pp. 155-197.

Terorotua, H., 2017. Impacts des événements extrêmes en Polynésie française et contribution à l'élaboration d'une typologie des îles coralliennes. Rapport de Master 2, La Rochelle University, STORISK project, 128 p.

Thieler, E.R., Himmelstoss, E.A., Zichichi, J.L., Ergul, A., 2009. The Digital Shoreline Analysis System (DSAS) Version 4.0: an ArcGIS extension for calculating shoreline change. USGS Open File Report, pp. 1–79 2008-1278.

Tou, J.T., R. C. Gonzalez, 1974. Pattern Recognition Principles, Addison-Wesley Publishing Company, Reading, Massachusetts. https://doi.org/10.1002/zamm.19770570626

Tuck, M., Kench, P. S., Ford, M.R., Masselink, G., 2019. Physical modelling of the response of reef islands to sea level rise. Geology 47(9), 803-806. http://dx.doi.org/10.1130/G46362.1.

641 Tucker C.J., 1979. Red and photographic infrared linear combinations for monitoring vegetation.
642 Remote Sens. Environ. 8, 127-150.
643 Wadey, M., Brown, S., Nicholls, R. J., Haigh, I., 2017. Coastal flooding in the Maldives: an
644 assessment of historic events and their implications. Nat. Haz. 89 (1), 131-159.
645 http://dx.doi.org/ 10.1007/s11069-017-2957-5.
646 Woodroffe, C. D., 1983. The impact of cyclone Isaac on the coast of Tonga. Pacific Science 37(3),
647 181-210.
648 Yates, M.L., Le Cozannet, G., Garcin, M., Salai, E., Walker, P., 2013. Multi-decadal atoll shoreline
649 change on Manihi and Manuae, French Polynesia. Journal of Coastal Research 29, 870–892.
650 http://dx.doi.org/10.2112/JCOASTRES-D-12-00129.1.
651
652